Ab Initio MRD–CI Study of the Spectrum of the TeO Molecule Employing Relativistic Effective Core Potentials †

4 AUTHORS, INCLUDING:

Vidisha Rai-Constapel
Heinrich-Heine-Universität Düsseldorf
16 PUBLICATIONS **64** CITATIONS

SEE PROFILE

Heinz-Peter Liebermann
Bergische Universität Wuppertal
136 PUBLICATIONS **1,278** CITATIONS

SEE PROFILE

Ab Initio MRD-CI Study of the Spectrum of the TeO Molecule Employing Relativistic Effective Core Potentials[†]

Vidisha Rai-Constapel,* Heinz-Peter Liebermann, and Robert J. Buenker

Fachbereich C-Mathematik und Naturwissenschaften, Bergische Universität Wuppertal, Gaussstr. 20, D-42119 Wuppertal, Germany

Sachchida N. Rai

Computer Centre, Bijni Complex, North-Eastern Hill University, Shillong-793003, Meghalaya, India

Received: May 9, 2005; In Final Form: June 21, 2005

Potential energy curves and properties of the low-lying electronic states of tellurium oxide have been computed using a configuration interaction treatment that includes the spin−orbit coupling interaction. Relativistic effective core potentials (RECPs) are used to describe the inner shells of both the Te and O atoms. Good agreement is obtained for the spectroscopic constants of the $X_1-X_2{}^3\Sigma^-$, $a^1\Delta$, and $b^1\Sigma^+$ states for which experimental data are available. The ratio of the parallel and perpendicular b−X transition moments, as well as the radiative lifetime of the b state, was computed, and both results were also found to be in good agreement with measurement. The energetic order of the electronic states in TeO appears to be very similar to that observed for the isovalent O_2 molecule, but the Rydberg valence-mixing effects that are so prominent in the latter's spectrum (e.g., for the Schumann−Runge bands) are totally absent in TeO.

I. Introduction

The goal of performing electronic structure calculations for molecules containing atoms of high nuclear charge at a level of accuracy comparable to that of lighter systems was greatly aided by the development of relativistic effective core potentials (RECPs).[1−5] As a result, it became much more practical to compute the potential energy surfaces and properties of systems containing heavy atoms that could be meaningfully compared to analogous results obtained for lighter molecules with the same number of valence electrons. A route was also opened for obtaining reliable predictions of fundamentally relativistic effects such as spin−orbit splittings and partial lifetimes for spin-forbidden processes that are common in the electronic spectra of molecules containing heavy atoms.

Experimental investigations of the electronic spectra of such molecules have provided an important stimulus for the development of the above theoretical methods. It is necessary to employ highly correlated wave functions that are of similar accuracy over a wide range of internuclear distances to describe excited electronic states with sufficient accuracy to be useful in the interpretation of the spectral data. The multireference single- and double-excitation configuration interaction (MRD-CI) method[6,7] has proven to be an effective means of achieving this goal. Adaptation of this technique to include scalar relativistic effects in the molecular Hamiltonian was a relatively simple task, but it was more difficult to maintain the same level of accuracy when spin-dependent operators were taken into consideration. Progress on the development of spin−orbit CI methods to achieve this goal has recently been reviewed,[8] and this work has shown that atoms in the intermediate range ($Z = 30-50$) can be effectively treated by means of a two-step procedure. The latter employs conventional large-scale CI wave functions as the basis for a compact matrix representation of the spin−orbit Hamiltonian.

The latter approach will be implemented in the present work to compute spin−orbit CI wave functions for tellurium oxide, TeO. This system is isoelectronic with the oxygen molecule and is known to possess a $^3\Sigma^-$ ground state with a $\pi^4\pi^{*2}$ electronic configuration. Fink et al.[9,10] reported experimental investigations of the spectrum of this molecule, and they were able to measure the spin splitting of the above triplet state as well as the location of the second excited state, the $b^1\Sigma^+$ of the same electronic configuration. The corresponding $a^1\Delta$ state has also been identified recently.[11] These authors also measured the partial lifetimes of the transitions of the $b^1\Sigma^+$ state to both components of the spin−split triplet ground state. In contrast to the situation for many other O_2-type systems, it was found that the perpendicular transition is stronger than the parallel transition for TeO.

Generally, one would like to have a detailed comparison of the more highly excited states of these two molecules. In O_2, a number of states with a $\pi^3\pi^{*3}$ electronic configuration are known, for example. One of these states is responsible for the Schumann−Runge bands, the $B^3\Sigma_u^-$. Early calculations[12,13] with the MRD-CI method showed that there is a strongly avoided crossing between this valence state and one of predominantly Rydberg character that produces an adiabatic potential with an unusually small equilibrium internuclear distance. A spin−orbit CI treatment has therefore been carried out for the TeO system to obtain a quantitative comparison of its electronic structure with that of O_2, as well as provide reliable predictions to aid researchers in future investigations of its molecular spectrum.

II. Theoretical Method

The 16-electron RECP reported by La John et al.[14] has been employed to describe the inner shells of the Te atom. The

---

[†] Part of the special issue "Donald G. Truhlar Festschrift".
* E-mail: vidi_shal@yahoo.com.

Ab Initio MRD-CI Study of TeO

J. Phys. Chem. A, Vol. 110, No. 2, 2006 **405**

(11s11p14d1f)/[9s8p6d1f] basis set from a previous all-electron TeO study[15] has been used to describe the valence shells. The large-exponent Gaussian exponents of the original basis set have not been included in the present calculations because they are used predominantly to describe the inner shells of tellurium and thus are not needed when an RECP is employed. The basis set was augmented by one d polarization function and one f polarization function with optimized exponents of 0.4 and 2.0 a_0^{-2}, respectively. The corresponding basis set for the oxygen atom has also been taken from ref 15 but is augmented by two d functions and one f function with optimized exponents of 0.9, 0.3, and 0.9 a_0^{-2}, respectively. The resulting basis set is (5s5p2d1f) /[4s3p2d1f] and is also used in conjunction with an RECP for the oxygen 1s shell.[16]

The first step in the theoretical treatment is to carry out SCF calculations at a series of internuclear distances for TeO in its $^3\Sigma^-$ ground state with a $\sigma^2\pi^4\pi^{*2}$ electronic configuration, the same as that of the oxygen molecule. The symmetry-adapted molecular orbitals thus obtained are used to construct the configurations to be used in the ensuing configuration interaction calculations without inclusion of the spin−orbit operator (Λ−S level of treatment). Details of these MRD-CI calculations are given in Table 1 for the equilibrium bond length of the TeO ground state ($r_e = 3.50\ a_0$). These calculations were performed in formal C_{2v} symmetry, but the one-electron basis set employed to construct the various configurations nevertheless transforms according to the irreducible representations of the linear $C_{\infty v}$ point group. A configuration selection procedure[6,17] was employed to limit the size of the CI secular equations in each case; a selection threshold of $T = 0.5 \times 10^{-6}\ E_h$ has been used for this purpose. The number of roots obtained in each case was chosen to be large enough to take into proper account the effects of higher-lying states in the final spin−orbit CI treatment for the states of major interest in the present study. For each of the $^3A_2$, $^1A_1$, and $^1A_2$ symmetries, nine roots have been calculated. For the other singlet, triplet, and quintet symmetries, the number of roots treated lies between two and five.

The leading electronic configurations for the lowest roots of each symmetry are also listed in Table 1. For the symmetries with 5−9 roots, the generated configuration space is on the order of $(25-35) \times 10^6$ SAFs (symmetry-adapted functions), while for symmetries with 2−4 roots, the corresponding order is $(12-19) \times 10^6$ SAFs. The configuration spaces are generated from 35 to 175 reference configurations depending on the Λ−S symmetry. At the above threshold, 47 000−120 000 SAFs are ultimately included in the final secular equations. The multi-reference Davidson correction,[18−20] which takes into account the effects of higher than double excitations with respect to the reference configurations, has been applied to the extrapolated ($T = 0$) energies of each root to estimate the energies at the full CI (AO basis limit) level of treatment. The Σc_p^2 values over the reference configurations in the CI eigenvectors fall in the 91−93% range (Table 1). The 4d electrons of the Te atom have been treated as a frozen core in the CI and the subsequent spin−orbit calculations. Hence, only 12 electrons are available for the excitation process. The calculations have been carried out for the range of internuclear distance between $r = 2.9$ and 9.5 a_0.

The Λ−S eigenfunctions are then used as basis for the final spin−orbit CI calculations (LSC−SO−CI [8]). The resulting spin-mixed functions are then combined with the Λ−S transition moments to obtain the corresponding Ω-state electronic transition moments at each value of r. The Numerov−Cooley numerical integration procedure[21,22] has been employed to solve

TABLE 1: Technical Details of the MRD-CI Calculations of $^{130}\text{Te}^{16}\text{O}^a$
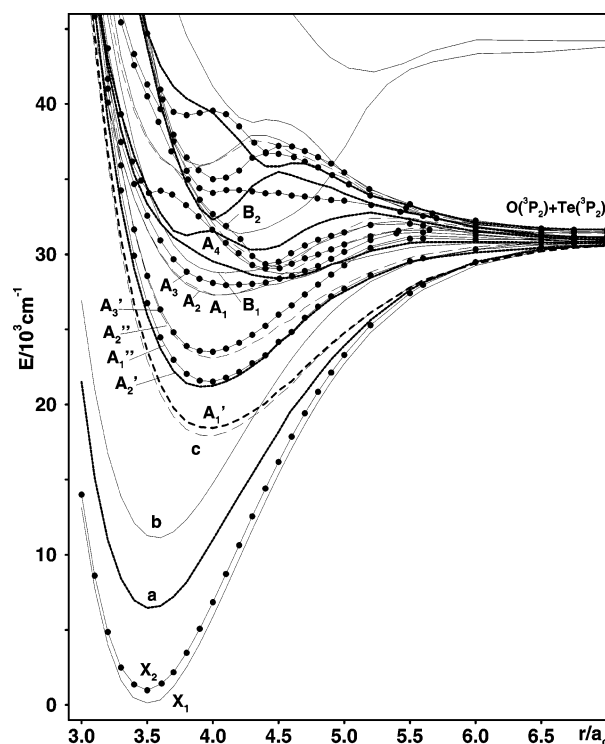
C_{2v}	N_{ref}/N_{root}	SAFTOT/SAFSEL	$C_{\infty v}$	leading configuration	Σc_p^2
$^3A_2$	99/8	35498152/115764	$1^3\Sigma^-$	$\sigma^2\pi^4\pi^{*2}$	0.931
			$1^3\Delta$	$\sigma^2\pi^3\pi^{*3}$	0.936
			$2^3\Sigma^-$	$\sigma^2\pi^3\pi^{*3}$	0.931
			$3^3\Sigma^-$	$\sigma\pi^4\pi^{*2}\sigma^*$	0.925
			$2^3\Delta$	$\sigma\pi^4\pi^{*2}\sigma^*$	0.924
			$4^3\Sigma^-$	$\sigma^2\pi^2\pi^{*4}$	0.919
			$5^3\Sigma^-$	$\sigma\pi^4\pi^{*2}\sigma^*$	0.914
			$6^3\Sigma^-$	$\sigma\pi^3\pi^{*3}\sigma^*$	0.919
$^3A_1$	58/4	19091314/69749	$1^3\Delta$	$\sigma^2\pi^3\pi^{*3}$	0.936
			$1^3\Sigma^+$	$\sigma^2\pi^3\pi^{*3}$	0.935
			$2^3\Delta$	$\sigma\pi^4\pi^{*2}\sigma^*$	0.914
			$2^3\Sigma^+$	$\sigma\pi^4\pi^{*2}\sigma^*$	0.913
$^3B_{1,2}$	81/5	24665880/95281	$1^3\Pi$	$\sigma^2\pi^4\pi^*\sigma^*$	0.924
			$2^3\Pi$	$\sigma\pi^4\pi^{*3}$	0.926
			$3^3\Pi$	$\sigma^2\pi^3\pi^{*2}\sigma^*$	0.927
			$4^3\Pi$	$\sigma^2\pi^3\pi^{*2}\sigma^*$	0.929
			$5^3\Pi$	$\sigma^2\pi^3\pi^{*2}\sigma^*$	0.929
$^1A_1$	175/9	32006437/106730	$1^1\Delta$	$\sigma^2\pi^4\pi^{*2}$	0.933
			$1^1\Sigma^+$	$\sigma^2\pi^4\pi^{*2}$	0.933
			$2^1\Delta$	$\sigma^2\pi^3\pi^{*3}$	0.930
			$2^1\Sigma^+$	$\sigma^2\pi^3\pi^{*3}$	0.929
			$3^1\Sigma^+$	$\sigma^2\pi^4\sigma^{*2}$	0.911
			$4^1\Sigma^+$	$\pi^4\pi^{*4}$	0.918
			$3^1\Delta$	$\sigma^2\pi^2\pi^{*4}$	0.916
			$4^1\Delta$	$\sigma\pi^4\pi^{*2}\sigma^*$	0.903
			$5^1\Sigma^+$	$\sigma\pi^4\pi^{*2}\sigma^*$	0.904
$^1A_2$	147/9	30034414/112981	$1^1\Delta$	$\sigma^2\pi^4\pi^{*2}$	0.931
			$1^1\Sigma^-$	$\sigma^2\pi^3\pi^{*3}$	0.935
			$2^1\Delta$	$\sigma^2\pi^3\pi^{*3}$	0.932
			$2^1\Sigma^-$	$\sigma\pi^4\pi^{*2}\sigma^*$	0.925
			$3^1\Delta$	$\sigma^2\pi^2\pi^{*4}$	0.920
			$4^1\Delta$	$\sigma\pi^4\pi^{*2}\sigma^*$	0.912
			$3^1\Sigma^-$	$\sigma^2\pi^3\pi^{*3}\sigma^{*2}$	0.921
			$4^1\Sigma^-$	$\sigma^2\pi^3\pi^{*3}\sigma^{*2}$	0.920
			$5^1\Sigma^-$	$\sigma\pi^3\pi^{*3}\sigma^*$	0.923
$^1B_{1,2}$	81/5	13051907/78532	$1^1\Pi$	$\sigma\pi^4\pi^{*3}$	0.927
			$2^1\Pi$	$\sigma^2\pi^4\pi^*\sigma^*$	0.920
			$3^1\Pi$	$\sigma^2\pi^3\pi^{*2}\sigma^*$	0.923
			$4^1\Pi$	$\sigma^2\pi^3\pi^{*2}\sigma^*$	0.929
			$5^1\Pi$	$\sigma^2\pi^3\pi^{*2}\sigma^*$	0.927
$^5A_1$	35/3	12860861/74446	$1^5\Delta$	$\sigma\pi^3\pi^{*3}\sigma^*$	0.922
			$1^5\Sigma^+$	$\sigma\pi^3\pi^{*3}\sigma^*$	0.921
			$2^5\Sigma^+$	$\sigma^2\pi^2\pi^{*2}\sigma^{*2}$	0.923
$^5A_2$	43/2	13081053/54208	$1^5\Sigma^-$	$\sigma\pi^4\pi^{*2}\sigma^*$	0.926
			$1^5\Delta$	$\sigma\pi^3\pi^{*3}\sigma^*$	0.923
$^5B_{1,2}$	41/2	14161701/47014	$1^5\Pi$	$\sigma^2\pi^3\pi^{*2}\sigma^*$	0.931
			$2^5\Pi$	$\sigma^2\pi^2\pi^{*3}\sigma^*$	0.905

^{a} The number of selected SAFs and the Σc_p^2 values over the reference configurations are given for $r = 3.50\ a_0$. SAFTOT designates the total number generated, SAFSEL is the number of selected SAFs, and N_{ref} and N_{root} refer to the number of reference configurations and roots treated, respectively.

the nuclear Schrödinger equations to obtain the corresponding vibrational energies and wave functions. Radiative lifetimes are obtained for each vibrational level by summing the Einstein coefficients for each of its downward transitions and inverting them.

III. Discussion of the Results

III.A. Potential Energy Curves. There are 18 Λ−S states that correlate with the lowest dissociation limit for the TeO molecule, Te (^3P) + O (^3P), and each of these potential curves has been calculated at the MRD-CI level of treatment (Figure 1). The next lowest asymptote is Te (^1D) + O (^3P), which correlates with nine other triplet states, and these potential curves are also shown in the diagram. The ground state and the two

406 *J. Phys. Chem. A, Vol. 110, No. 2, 2006*

Rai-Constapel et al.

Figure 1. Computed MRD-CI potential energy curves for the low-lying electronic states of the TeO molecule obtained at the $\Lambda-S$ level of treatment, excluding the spin–orbit coupling interaction.

Figure 2. Computed spin–orbit CI potential energy curves for the low-lying electronic states of the TeO molecule.

lowest excited states of TeO are derived from the same electronic configuration of $\sigma^2\pi^4\pi^{*2}$. They correlate to the first dissociation limit of Te (^{3}P) + O (^{3}P). At the equilibrium distance of the $X^3\Sigma^-$ ground state ($r_e = 3.50$ a_0), the total weight of the reference configurations for each of the three lowest-lying states, X, $a^1\Delta$, and $b^1\Sigma^+$, is ca. 93%. The contribution of the $\sigma^2\pi^4\pi^{*2}$ electronic configuration to the ground state wave function is 86%, while it is only 82% for the $a^1\Delta$ state and 77% for the $b^1\Sigma^+$ state. The other major contributions for the b state come from the $\sigma^2\pi^3\pi^{*3}$ and $\sigma^2\pi^2\pi^{*4}$ electronic configurations.

In the Franck–Condon (FC) region of the ground state, the π orbital is mainly concentrated on the oxygen atom while the π^* molecular orbital (MO) is localized on the tellurium atom, as one would expect on the basis of electronegativity considerations. As a consequence, there are considerably fewer differences in their bonding characteristics than there are for the lighter O_2 molecule. The potential minima for the above three states therefore occur at very nearly the same bond distance, despite the rather significant differences in the respective occupations of these two MOs (Figure 1). The next three states are predominantly $\sigma^2\pi^3\pi^{*3}$ in character ($c^1\Sigma^-$, $A'^3\Delta$, and $A''^3\Sigma^+$), however, and their equilibrium bond distances are notably larger, reflecting the fact that the π^* MO is somewhat more antibonding than the π MO in TeO. The same energetic order is observed for these states in the O_2 molecule,[23] emphasizing the very close relationship that exists between these two isovalent systems. The next lowest state at the ground-state r_e value is the $A^3\Pi$ with a $\sigma^2\pi^4\pi^*\sigma^*$ configuration. Its potential minimum occurs at a slightly larger bond distance than the previous three states, suggesting that the π MO is somewhat less bonding than the σ MO in TeO. Lying slightly above it (Figure 1) is the next state of predominantly $\sigma^2\pi^3\pi^{*3}$ character, the $B^3\Sigma^-$. It has nearly the same bond length as the c, A′, and A″ states, but it dissociates to a higher atomic limit, Te (^{1}D),

again similarly to that in O_2, for which this electronic state is responsible for the Schumann–Runge band system.[23] The lowest quintet state ($^5\Pi$) of TeO is also found in this region of the spectrum. It has the largest bond length and smallest binding energy of the low-lying states of this molecule and dissociates to the atomic ground state.

The next step in the theoretical treatment is to include the spin–orbit interaction in the molecular Hamiltonian. The $\Lambda-S$ MRD-CI wave functions are then employed as a contracted basis for this Hamiltonian, as discussed in section II, and the resulting potential curves are shown in Figure 2. A total of 50 Ω states are obtained from the 18 $\Lambda-S$ states that correlate with the Te (^{3}P) + O (^{3}P) atomic ground state of this system: 10 states of 0^+, 9 of 0^-, 16 of 1, 10 of 2, 4 of 3, and 1 of $\Omega = 4$ symmetry in the double group of $C_{\infty v}$. Potential curves have been computed for all of these electronic states, but some of the repulsive higher-lying states have been omitted from Figure 2 for clarity purposes.

The effect of the spin–orbit coupling is not large enough to greatly modify the general appearance of the potentials relative to Figure 1. The main distinctions are simply the result of splitting the pure spin-states into their Ω components. The computed D_e value for the ground-state $X_1{}^3\Sigma^-_{0+}$ is obtained from calculations at $r = 9.5$ a_0 and is found to be 30 700 cm^{-1}. The SO interaction lowers the dissociation energy by 1920 cm^{-1} relative to that obtained at the $\Lambda-S$ level of treatment. No experimental value for this quantity is as yet available. The above result was obtained by averaging the various spin components of the Te (^{3}P) + O (^{3}P) asymptote. It may be compared with the corresponding value for the TeF molecule,[24] 25 480 cm^{-1}. The latter value is 5220 cm^{-1} smaller than the present computed result for TeO, which is at least qualitatively consistent with the fact that Te is bound by a double bond in this system as opposed to a single bond in TeF.

III.B. Spectroscopic Constants. The computed Ω-state potential energy curves have been employed to obtain predictions for the adiabatic transition energies (T_e) of the low-lying

Ab Initio MRD-CI Study of TeO

J. Phys. Chem. A, Vol. 110, No. 2, 2006 **407**

TABLE 2: Calculated (This Work) and Experimental Spectroscopic Properties of $^{130}Te^{16}O$ (Transition Energies, T_e, Bond Length, r_e, and Vibrational Frequencies, ω_e)

state	T_e (cm^{-1}) calcd	T_e (cm^{-1}) exptl	r_e (Å) calcd	r_e (Å) exptl	ω_e (cm^{-1}) calcd	ω_e (cm^{-1}) exptl
$X_1^3\Sigma_{0+}^-$	0	–	1.842	–	802	797.11[25]
$X_2^3\Sigma_1^-$	923	782.4[10]	1.841	–	801	798.06[25]
$a^1\Delta_2$	6448	5247[11]	1.863	–	736	–
$b^1\Sigma_{0+}^+$	11253	9961.5[10]	1.882	–	704	726[9]
$c^1\Sigma_{0-}^-$	17841	–	2.095	–	505	–
$A_1'^3\Delta_3$	18296	–	2.105	–	503	–
$A_2'^3\Delta_2$	21089	–	2.093	–	518	–
$A_1''^3\Sigma_1^+$	21435	–	2.102	–	502	–
$A_2''^3\Sigma_{0-}^+$	23051	–	2.113	–	480	–
$A_3'^3\Delta_1$	23417	–	2.098	–	500	–
$B^3\Sigma_{10+}^-$	–	–	2.270	–	305	–
$B_2^3\Sigma_1^-$	–	–	2.332	–	393	–

states of TeO as well as their equilibrium bond lengths, r_e, and vibrational frequencies, ω_e. These results are given in Table 2. The fine structure splitting for the $X^3\Sigma^-$ ground state is computed to be 923 cm^{-1}, as compared to the experimental value of 782.4 cm^{-1}.[9,10] The overestimation of 141 cm^{-1} is most probably caused by inaccuracies in the RECP employed for the Te atom,[14] but is still a considerable improvement over the previous all-electron result of only 473 cm^{-1} [15] obtained with the Breit–Pauli Hamiltonian. The experimental T_e value for the $a^1\Delta$ state is 5247 cm^{-1} [9]. The present computed value is 6448 cm^{-1}, which is in very good agreement with the previous theoretical estimate[15] of 6329 cm^{-1}. There is also an observed T_e value for the $b^1\Sigma^+$ state, 9926.2 cm^{-1}.[9,10] This result is overestimated in the calculations by 1327 cm^{-1} or 0.16 eV, which is very close to the error in the calculated $a^1\Delta$ transition energy. The fact that both computed values are too large by this amount is consistent with previous experience with ab initio CI calculations and also the fact that the correlation energy for the singlet a and b states are expected to be larger than for the X state because of the latter's triplet multiplicity.

The calculated equilibrium bond lengths for these states become larger with increasing excitation energy (Table 2). This effect is expected because of the fact that all these states correlate with the same dissociation limit. Comparable variations in the computed vibrational frequencies are also found (i.e., they decrease in going from the X to the a and b states). There is an experimental value for the b state's frequency.[9] The computed result underestimates it by 22 cm^{-1} or 3%.

There is an energy gap of 6600 cm^{-1} between the b and c states. Transitions from the latter to the X ground state are quite weak, as will be discussed in the next section. The next group of states are derived primarily from the same $\sigma^2\pi^3\pi^{*3}$ configuration but are of higher multiplicity than c. The $A'^3\Delta$ is split into three components, with $\Omega = 3$ lying the lowest. The spin splittings between the following components are 2793 cm^{-1} and 2328 cm^{-1}, respectively, notably larger than the corresponding value for the two X components. The $\Omega = 2$ and 1 states are separated from one another by the two intervening components of the $A''^3\Sigma^+$ state (Table 2). The latter are separated by only 1616 cm^{-1}, although this value is still larger than the X state's fine structure splitting.

The bond lengths of the c, A', and A'' states are computed to be quite similar, and they are also notably larger than those for the lower-energy group of states. Both of these characteristics are consistent with their common electronic configuration and the fact that the π^* MO is triply occupied in this case. The computed vibrational frequencies all lie in the 500 cm^{-1} range,

about 200 cm^{-1} smaller than for the b state, consistent with the above results for the bond lengths.

III.C. Transition Moments and Radiative Lifetimes. The composition of the low-lying spin-states of the TeO molecule is given in Table 3. This information is quite important for the interpretation of the computed transition moment data. The partial and total radiative lifetimes corresponding to these states are given in Table 4. The $X_2–X_1$ transition between the ground state components is found to be extremely weak, consistent with the fact that it has never been observed experimentally. The fine structure splitting mentioned above is obtained as the difference between the $b–X_2$ and $b–X_1$ transitions.[9] The lifetime of the X_2 state is computed to be 19.2 s. The fact that there is even this amount of instability can be traced to the small admixture of the $b^1\Sigma^+$ state in the X_1 ground state wave function (see Table 3). The contribution of the latter grows steadily with increasing r, but it is still rather small at the equilibrium bond length. The computed values of the various transition moments of interest are shown in Figures 3–4.

The lifetime of the $a^1\Delta$ state is several hundred times shorter, but it is still nearly 100 ms. It is easily understandable from this result that downward transitions were very difficult to detect from this state, despite intensive efforts to do so.[9] They become weakly allowed because of the admixture of a $^3\Pi$ state in its wave function (Table 3). The $a–X_2$ band has been detected recently.[11]

The lifetime of the $b^1\Sigma^+$ state has been measured.[9] There are both parallel and perpendicular transitions from it to the different spin components of the X ground state. The ratio of the corresponding transition moments has also been measured and has a value of μ_{par}/μ_{perp} of -0.425 [11] (note that $\mu_{perp} = 2^{0.5}\mu_x$). The sign is significant because it is phase independent. The computed ratio does have the correct sign (-0.4193) and is in good agreement with the measured value. The dependence of these two transition moments on the Te–O bond distance is also shown is Figure 3. The $b–X_2$ result gradually decreases in absolute value with r outside the FC region, whereas the $b–X_1$ value at first increases because of the greater mixing of the $^3\Sigma^-$ and $^1\Sigma^+$ Λ–S states in both the upper and lower Ω states. The fact that the above transition moment ratio is less than unity (in absolute value) in TeO is in contrast to the corresponding results for other systems that are isovalent with O_2. This behavior for the two transition moments demonstrates that this unusual result depends quite specifically on the value of the TeO equilibrium bond length in the $X^3\Sigma^-$ ground state.

The radiative lifetime for the b state is determined from the Einstein coefficients for both the parallel and perpendicular transitions. The partial lifetime for the parallel $b–X_1$ transition is double that for the perpendicular $b–X_2$ value (Table 4). The computed lifetime of the b state is 368 μs, which may be compared with the best experimental result obtained to date[10] of 700 ($+100$ or -50) μs. The latter error bars may not take into account all possible errors in the measurements and so the above agreement is considered to be quite satisfactory for such weak transitions.

The lifetimes of the next lowest group of states with $\sigma^2\pi^3\pi^{*3}$ character have also been calculated with the present wave functions. The relevant transition moment results are shown in Figure 4. The c state only has electric–dipole transitions to the X_2 state. They become allowed in the spin–orbit CI through the admixture of $^3\Pi$ character in the c state's wave function (Table 3). The computed lifetime is thus only in the millisecond range (Table 4). The next lowest spin state is the $A'^3\Delta_3$ state. It has spin-forbidden transitions to the $a^1\Delta_2$ state and has a

TABLE 3: Composition of Ω States of ^{130}Te^{16}O (c^2, %) at Various Bond Distances r [a]

state	r (a_0)	$^3\Sigma^-$	$^3\Sigma^+$	$^3\Pi$	$^3\Delta$	$^1\Sigma^-$	$^1\Sigma^+$	$^1\Pi$	$^1\Delta$	$^5\Pi$	$^5\Sigma^+$	$^5\Sigma^-$	$^5\Delta$
$X_1\,^3\Sigma_{0+}$	3.20	92.4					7.0						
	3.50[b]	90.7					8.4						
	4.00	86.4		1.2			11.6						
	4.20	83.6		1.8			13.7						
	4.30	81.7		2.0			15.1						
	5.00	61.4		4.4			30.2			3.3			
$X_2\,^3\Sigma_1$	3.20	99.4											
	3.50[b]	98.9											
	4.00	97.0	1.5										
	4.20	95.1	2.6							1.2			
	4.30	93.8	3.4							1.6			
	5.00	70.4	15.5	1.0	1.3					10.5			
$a^1\Delta_2$	3.20								99.0				
	3.50[b]				1.0				98.2				
	4.00			1.4	3.7				94.3				
	4.20			1.8	6.4				90.9				
	4.30			2.0	8.3				88.5				
	5.00			4.0[c]	24.7				67.2	2.5			
$b^1\Sigma_{0+}$	3.20	7.0					92.2						
	3.50[b]	8.5					90.4						
	4.00	12.0		1.2			85.8						
	4.20	14.2		1.8			82.6						
	4.30	15.7		2.2			80.5						
	5.00	19.8		11.4[c]			46.6			20.0			
$c^1\Sigma_{0-}$	3.20		23.4			75.3							
	3.50		26.7	1.0		71.8							
	4.00[b]		30.1	1.8[c]		66.9							
	4.20		31.0	2.0[c]		65.0							
	4.30		31.9	1.8[c]	1.0	63.5				1.2			
	5.00		33.2	3.0[c]	1.0	57.8				4.1			
$A_1'\,^3\Delta_3$	3.20				98.9								
	3.50				98.1					1.5			
	4.00[b]				95.6					3.7			
	4.20				93.6					5.3			
	4.30			1.0	92.3					6.4			
	5.00		1.5	1.0[c]	76.7					19.9			
$A_2'\,^3\Delta_2$	3.20			5.9	92.3								
	3.50			1.0	96.2				1.3[c]				
	4.00[b]				91.6				3.8	2.8			
	4.20		1.0		86.5				6.5	4.7			
	4.30		1.0		82.7				8.5	6.2			
	5.00		1.0	3.8	26.8				17.4	49.7			
$A_1''\,^3\Sigma_1^+$	3.20	3.9[c]	90.7	3.4				1.0					
	3.50	3.0[c]	94.1							1.1			
	4.00[b]	3.5[c]	92.0							3.1			
	4.20	4.5[c]	89.0							4.8			
	4.30	5.3[c]	86.9		1.0					6.0			
	5.00	7.3[c]	29.6	2.8	4.2					51.9			
$A_2''\,^3\Sigma_{0-}^+$	3.20		1.0	98.5									
	3.50		71.3			26.4							
	4.00[b]		64.7	1.2		30.3				3.1			
	4.20		60.0	2.5		30.9				5.6			
	4.30		56.2	3.5		31.4				7.8			
	5.00		16.1	16.8		20.8				42.2			
$A_3'\,^3\Delta_1$	3.20			91.9	2.0			4.9					
	3.50				98.5								
	4.00[b]				97.0					1.6			
	4.20				95.1					3.2			
	4.30			1.0	93.3					4.8			
	5.00	15.2	23.7	5.4	13.1					39.1			
$A_1\,^3\Pi_{0+}$	3.20	1.0		98.1									
	3.50	5.1[c]		92.7			1.2[c]						
	4.00[b]	7.9[c]		86.5			3.1[c]			1.6			
	4.20	2.5[c]		83.8			3.8[c]			8.8			
	4.30			73.1			4.3[c]			20.8			
	5.00	13.4		8.0[c]			12.5[c]			60.9	2.9[c]		
$A_2\,^3\Pi_{0-}$	3.20		73.2	2.5[c]		23.1							
	3.50			98.1		1.0							
	4.00[b]		1.0	95.0		1.2				2.2			
	4.20		2.4	90.1		2.2				4.3			
	4.30		4.0	85.0		3.0				6.8			
	5.00		38.1	5.7[c]		6.8				42.2		5.7	

Ab Initio MRD-CI Study of TeO

J. Phys. Chem. A, Vol. 110, No. 2, 2006 **409**

TABLE 3 (Continued)

state	r (a_0)	$^3\Sigma^-$	$^3\Sigma^+$	$^3\Pi$	$^3\Delta$	$^1\Sigma^-$	$^1\Sigma^+$	$^1\Pi$	$^1\Delta$	$^5\Pi$	$^5\Sigma^+$	$^5\Sigma^-$	$^5\Delta$
$A_3\,^3\Pi_1$	3.20			6.5^c	92.8								
	3.50	2.2^c		91.6				4.2^c					
	4.00^b	1.9^c		88.6				2.1		5.0			
	4.20			75.5	2.1			1.7		18.4			
	4.30			57.3	4.0			1.1		35.4			
	5.00			11.5^c	69.2^c			2.9^c		13.6^c		1.0	
$A_4\,^3\Pi_2$	3.20			92.3	5.1				1.0			1.3	
	3.50			95.2^c	1.0				1.4^c				
	4.00^b			84.4^c					1.1	12.0		1.3	
	4.20			41.2	2.7					53.7			
	4.30			21.9	4.7					71.0			
	5.00			14.6	35.7^c				3.4	41.4^c			2.3

^{a} Entries are only made for contributions with $c^2 \geq 1.0\%$. ^{b} An approximate equilibrium distance for this state. ^{c} Contributions from the higher-lying roots of this symmetry are included.

TABLE 4: Partial and Total Radiative Lifetimes (s) for Transitions from the $v' = 0$ Level of the $^{130}Te^{16}O$ Excited States to the $X_1\,^3\Sigma_{0+}^-$ (τ_1) and $X_2\,^3\Sigma_1^-$ (τ_2) States ^{b}

		τ_2		
state	τ_1	$\tau_\perp$	τ	τ_{tot}
$X_2\,^3\Sigma_1^-$	19.2			19.2
$a\,^1\Delta_2$		$87.8(-3)^a$		$52.4(-3)$
		$130(-3)$		
$b\,^1\Sigma_{0+}^+$	$1.1(-3)$	$550(-6)$		$368(-6)$
$c\,^1\Sigma_{0-}^-$		$1.4(-3)$		$1.4(-3)$
$A_1'\,^3\Delta_3 \rightarrow a\,^1\Delta_2$ ^{b}		$9.3(-3)$		$9.3(-3)$
$A_2'\,^3\Delta_2$		$1.9(-3)$		$1.9(-3)$
$A_3'\,^3\Delta_1$	$2.5(-3)$		$12.2(-3)$	$2.07(-3)$
$A_1''\,^3\Sigma_1^+$	$408(-6)$		$8.3(-6)$	$8.1(-6)$
$A_2''\,^3\Sigma_{0-}^+$		$1.2(-3)$		$1.2(-3)$

^{a} Numbers in parantheses indicate powers of ten. ^{b} Note that X_1 and X_2 are not the lower states in this case.
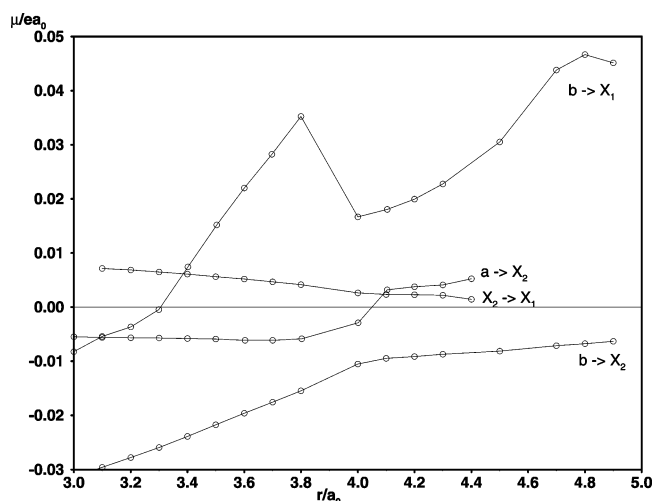

Figure 3. Computed electronic dipole transition moments between the $b\,^1\Sigma^+$, $a\,^1\Delta$, and X_1, $X_2\,^3\Sigma^-$ states as a function of Te−O internuclear distance. Note the difference in sign between the b−X_1 and b−X_2 values, which has been verified experimentally[9].

Figure 4. Computed electronic dipole transition moments between the various spin components of the $c\,^1\Sigma^-$, $A\,^3\Delta$, and $A\,^3\Sigma^+$ states of the TeO molecule and the X_1 and X_2 ground state multiplets.

lifetime an order of magnitude longer than that of the c state. The other two $^3\Delta$ spin components have somewhat shorter lifetimes, but they are still higher than a millisecond.

The situation is qualitatively different for the $\Omega = 1$ component of the $A''\,^3\Sigma^+$ state, but not for the corresponding $\Omega = 0$ component. A radiative lifetime of 8.1 μs has been computed for the former, which is primarily the result of parallel transitions to the X_1 ground state. The root cause is the admixture of $^3\Sigma^-$ character to the A'' spin state, in this case (Table 3). The $\Omega = 0$ c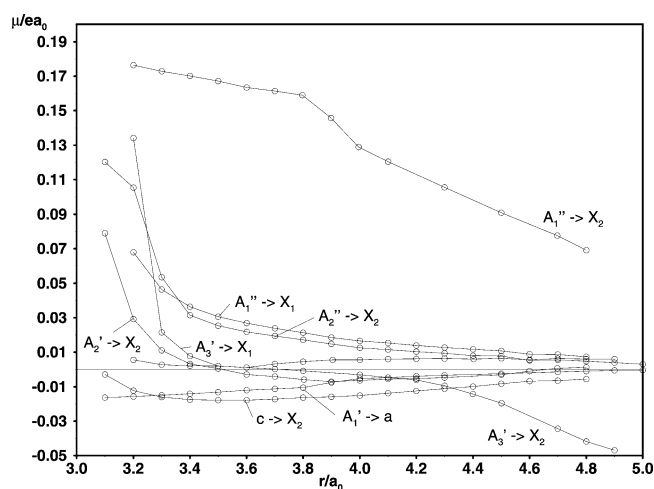omponent has 0^- symmetry and therefore cannot mix with the $^3\Sigma^-$ state. Instead, it has major contributions from the $c\,^1\Sigma^-$ and $^5\Pi$ states, neither of which has dipole-allowed transitions to either X_1 or X_2 (contributions to the Einstein coefficients for transitions to other low-lying states have not been considered in the above calculations).

III.D. Comparison with O_2. The close similarity between the Λ−S potential curves of the TeO system and those of O_2 has already been noted in the above discussion. There are nonetheless some major differences. The main cause of these distinctions is the lack of low-lying Rydberg states in the low-energy portion of the TeO spectrum. In O_2, the lowest $^3\Pi$ valence state in the FC region has an excitation energy of ca 9 eV, for example, whereas the lowest Rydberg state of the same symmetry has a potential minimum at only a slightly larger distance of ca 11 eV.[13] There is a strongly avoided crossing between these two states that causes an unusual shoulder in the lower adiabatic potential. No such effect is found for TeO because the analogous valence state has only a 4 eV excitation energy. As a result, the corresponding Rydberg states lie far too high in the TeO spectrum to produce a similar effect.

The computed Λ−S potential curves in this region of the TeO spectrum are shown in Figure 5. A comparison with the analogous theoretical data for the O_2 molecule (see Figure 3 of ref 13) shows that there is also another important difference. The excitation energy of the $A\,^3\Pi$ state in TeO is smaller than the dissociation energy of the ground state, whereas in O_2 the D_e value is at least 4 eV smaller than the adiabatic transition energy for the corresponding state. Consequently, once the aforementioned shoulder in the $O_2\,^3\Pi_u$ potential has been
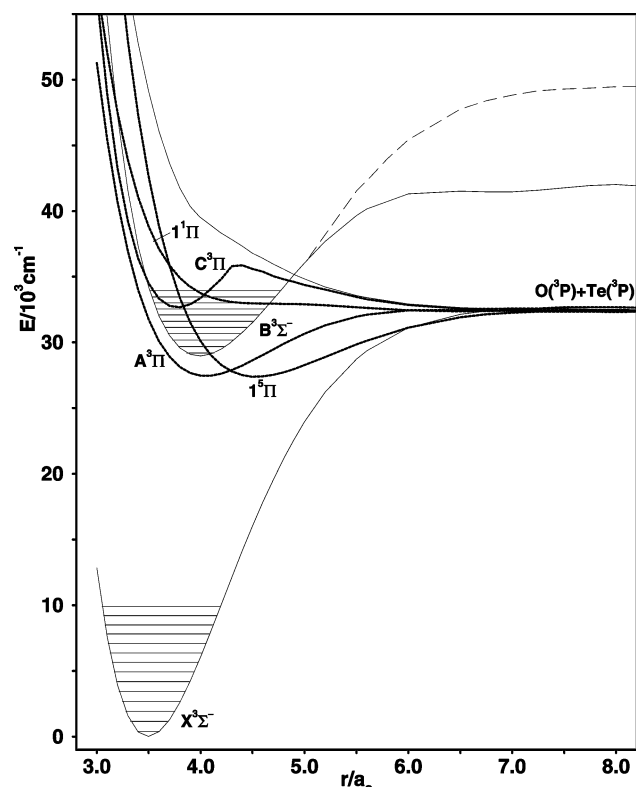
Figure 5. Computed $\Lambda-S$ potential curves for various low-lying states of the TeO molecule. Vibrational levels are also shown for the $X^3\Sigma^-$ and $B^3\Sigma^-$ states. Note that the latter dissociates to a higher atomic limit than most of the other states in the diagram.

reached, the energy for this state rapidly decreases as the bond distance is further increased.

One of the most prominent features in the O_2 spectrum is the Schumann−Runge continuum.[23] The upper state responsible for these absorption bands is the $B^3\Sigma_u^-$ state. It has been shown in earlier work[12,13] that there are two states of this symmetry that undergo a strongly avoided crossing similar to that mentioned above for the $^3\Pi_u$ states. The most interesting consequence of this Rydberg−valence interaction is the appearance of a second adiabatic state with a relatively short bond length and a vibrational frequency that corresponds to a triply bonded system. The absence of Rydberg diabatic states below 6 eV in the TeO spectrum negates any possibility of a similar occurrence in this case. The computed potential curve for the corresponding state ($B^3\Sigma^-$) looks very much like the diabatic valence $\sigma^2\pi^3\pi^{*3}$ state that had been expected for O_2 before the ab initio CI calculations became available. As for the latter molecule, it was found that this TeO $\Lambda-S$ state dissociates to an excited state of the atoms, Te (^1D) and O (^3P). One therefore expects a continuum in this region of the TeO spectrum similar to the well-known Schumann−Runge bands in the lighter system, but with no tightly bound upper state embedded in it.

The situation is complicated by the spin−orbit coupling interaction. As can be seen from Figure 2, there is a rather large difference between the potential curves for the respective $\Omega = 1$ and 0^+ spin components of the B state in TeO. The lower-energy component is $B_1\Sigma_{0+}^{3-}$, and it dissociates to the Te (^3P) + O (^3P) ground-state atomic limit rather than to Te (^1D). This fact causes a definite change in the curvature of this potential relative to its counterpart at the $\Lambda-S$ level of treatment so that it becomes far less tightly bound as a result. The potential curve of the B_2 state of $\Omega = 1$ symmetry is much more similar to the spin-independent potential of Figure 5, except for a weakly

avoided crossing that occurs near 5.0 a_0. These circumstances are reflected in the computed spectroscopic constants for the two states (Table 2). The equilibrium bond length for the $\Omega = 0^+$ component is 0.062 a_0 shorter than that for $\Omega = 1$, and the vibrational frequency of the latter is 88 cm^{-1} larger.

Conclusion

The electronic spectrum of tellurium oxide is found to differ from that of the isovalent oxygen molecule in a number of ways, although many similarities have also been found. Chief among these is the order of the electronic states in the low-energy region. With the aid of effective core potentials (RECPs), it has been possible to accurately describe key relativistic effects for the TeO molecule such as spin−orbit splittings and Einstein coefficients for spin-forbidden transitions by employing large-scale configuration interaction calculations. There is a tendency to overestimate singlet−triplet energy differences because of a well-known effect of the electron correlation. In the present calculations, the $b^1\Sigma^+$ and $a^1\Delta$ states are found to lie 0.15 and 0.16 eV, respectively, higher in energy relative to the $X_2^3\Sigma_1^-$ state than has been observed experimentally. This degree of regularity led to a prediction for the location of the previously undetected $a^1\Delta$ state that was only 125 cm^{-1} in error. The X_2-X_1 fine structure splitting is also overestimated in the present treatment (by 141 cm^{-1}), but this appears to have been caused primarily by deficiencies in the RECP employed for the Te atom. Each of the above four states dissociates to the same Te (^3P) + O (^3P) atomic limit, and as a result, there is a steady increase in the equilibrium bond length with excitation energy as well as a corresponding decrease in vibrational energy according to the calculations.

The b state undergoes much stronger mixing with the X_1 ground state in TeO than in O_2 because of the effects of spin−orbit coupling in the heavier system. Contrary to what might be expected, the b−X parallel transition moment is smaller than the perpendicular. The computed ratio of these two moments is found to be in quite good agreement, both in magnitude and sign, with that measured experimentally. The radiative lifetime for the b state is calculated to 368 μs, which is roughly one-half of the corresponding measured value of 700 ± 100 μs.[10] This is considered to be good agreement in light of the difficulties inherent in the experimental determination of the Einstein coefficients for such weakly allowed transitions.

The magnitude of the spin−orbit interaction in TeO is sufficient to cause the $A'^3\Delta$ state to split apart so widely that the $A''^3\Sigma^+$ state is found to lie between its $\Omega = 2$ and 1 components, quite unlike the situation in O_2. Each of these multiplets and the $c^1\Sigma^-$ state have nearly the same equilibrium bond length, all of which are more than 0.2 a_0 larger than for the lower-lying X, a, and b states discussed first. This is because they result from a $\pi-\pi^*$ transition relative to the TeO ground state. The resulting increase in bond distance is considerably smaller than the corresponding value for the O_2 molecule, which shows a clear difference in the electronic structure of these two systems. Because of the relatively large difference in the electronegativities of the Te and O atoms, the bonding−antibonding characteristics of the π and π^* MOs are notably less protracted in TeO than in O_2, which helps to minimize the changes in bond length upon $\pi-\pi^*$ excitation in the former system. All of these higher-lying states are computed to have radiative lifetimes in the millisecond range with the lone exception of the Σ_1^{3+} state.

Perhaps the most notable difference between TeO and O_2 is the lack of Rydberg−valence mixing in the heavier system. This

Ab Initio MRD-CI Study of TeO

J. Phys. Chem. A, Vol. 110, No. 2, 2006 **411**

is primarily caused by the fact that the valence states discussed above are more densely packed in TeO, whereas the ionization potentials of the two systems do not differ by a large amount. The second state of $^3\Sigma_u^-$ symmetry in O_2 has been found to possess a relatively short equilibrium distance because of the Rydberg−valence mixing in this system, and it is observed within the Schumann−Runge continuum. A corresponding strongly avoided crossing is absent for TeO. The valence state closely resembles the lowest diabatic state of the above symmetry in O_2, and it dissociates to Te (^{1}D) when the spin−orbit interaction is omitted from the theoretical treatment. Its potential curve does not possess a shoulder because the above dissociation limit lies above the potential minimum, unlike the case for its counterpart in O_2. When the spin−orbit interaction is included, the lowest component of the B$^3\Sigma^-$ state is found to dissociate to the ground Te (^{3}P) asymptote, thereby producing a much flatter potential curve than at the Λ−S level of treatment. The upper spin component (B$_2$$^3\Sigma_1^-$) has a much deeper potential well because it dissociates to the higher Te (^{1}D) atomic limit.

References and Notes

(1) Kahn, L. R.; Baybutt, P.; Truhlar, D. G. *J. Chem. Phys.* **1976**, *65*, 3826.

(2) Lee, Y. S.; Ermler, W. C.; Pitzer, K. S. *J. Chem. Phys.* **1977**, *67*, 5861.

(3) Christiansen, P. A.; Lee, Y. S.; Pitzer, K. S. *J. Chem. Phys.* **1979**, *71*, 4445.

(4) Ermler, W. C.; Lee, Y. S.; Christiansen, P. A.; Pitzer, K. S. *Chem. Phys. Lett.* **1981**, *81*, 70.

(5) Hafner, P.; Schwarz, W. H. E. *Chem. Phys. Lett.* **1979**, *65*, 537.

(6) Buenker, R. J.; Peyerimhoff, S. D. *Theor. Chim. Acta* **1974**, *35*, 33.

(7) Buenker, R. J.; Peyerimhoff, S. D. *Theor. Chim. Acta* **1975**, *39*, 217.

(8) Alekseyev, A. B.; Liebermann, H.-P.; Buenker, R. J. In *Recent Advances in Relativistic Molecular Theory*; Hirao, K., Ishikawa, Y. Eds.; World Scientific: Singapore, 1999; p 1.

(9) Winter, R.; Barnes, I.; Fink, E. H.; Wildt, J.; Zabel, F. *J. Mol. Struct.* **1982**, *80*, 75.

(10) Setzer, K. D. Ph.D. Thesis, Wuppertal, 1991**.**

(11) Fink, E. H. Private communication.

(12) Buenker, R. J.; Peyerimhoff, S. D. *Chem. Phys.* **1975**, *8*, 324.

(13) Buenker, R. J.; Peyerimhoff, S. D. *Chem. Phys. Lett.* **1975**, *34*, 225.

(14) LaJohn, L. A.; Christiansen, P. A.; Ross, R. B.; Atashroo, T.; Ermler, W. C. *J. Chem. Phys.* **1987**, *87*, 2812.

(15) Rai, S. N.; Buenker, R. J. *J. Chem. Phys.* **1990**, *147*, 327.

(16) Pacios, L. F.; Christiansen, P. A. *J. Chem. Phys.* **1985**, *82*, 2664.

(17) Krebs, S.; Buenker, R. J. *J. Chem. Phys.* **1995**, *103*, 5613.

(18) Davidson, E. R. In *The World of Quantum Chemistry*; Daudel, R., Pullman, B., Eds.; Reidel: Dordrecht, The Netherlands, 1974; p 17.

(19) Hirsch, G.; Bruna, P. J.; Peyerimhoff, S. D.; Buenker, R. J. *Chem. Phys. Lett.* **1977**, *52*, 442.

(20) Knowles, D. B.; Alvarez-Collado, J. R.; Hirsch, G.; Buenker, R. J. *J. Chem. Phys.* **1990**, *92*, 585.

(21) Cooley, J. W. *Math. Comput.* **1961**, *15*, 363.

(22) Peric, M.; Runau, R.; Römelt, J.; Peyerimhoff, S. D.; Buenker, R. J. *J. Mol. Spectrom.* **1979**, *78*, 309.

(23) Krupenie, P. H. *J. Phys. Chem. Ref. Data* **1972**, *1*, 423.

(24) Rai, V.; Liebermann, H.-P.; Alekseyev, A. B.; Buenker, R. J. *J. Chem. Phys.* **2001**, *114*, 8386.

(25) Huber, K. P.; Herzberg, G. *Molecular Spectra and Molecular Structure Constants of Diatomic Molecules,* 1979; p. 638.